Vaccine 37 (2019) 1073–1079

Contents lists available at ScienceDirect

Vaccine

journal homepage: www.elsevier.com/locate/vaccine

Preparation-free method can enable rapid surfactant screening during industrial processing of influenza vaccines

Ziya Sahin [a], Ronald Neeleman [b], Jonathan Haines [b], Veysel Kayser [a,*]

[a] School of Pharmacy, Faculty of Medicine and Health, The University of Sydney, Sydney, Australia
[b] Viral Technology, MTech, Sanofi-Pasteur, Swiftwater, USA

ARTICLE INFO

Article history:
Received 26 June 2018
Received in revised form 24 December 2018
Accepted 30 December 2018
Available online 23 January 2019

Keywords:
Influenza split-virus vaccine
Rapid Triton X-100 screening
UV–Vis absorption spectroscopy
Biopharmaceutical formulation safety
Protein aggregation

ABSTRACT

Triton X-100 (TX-100) is the most common surfactant used to split viruses during the production of influenza split-virus vaccines. It is a mild surfactant not known to denature the viral proteins; this property makes TX-100 useful for maintaining antigen conformational structure, and, as an added benefit, for partially stabilizing vaccine formulations against protein aggregation. Despite its benefits, TX-100 needs to be filtered out after virus splitting has been achieved, due to its toxicity in large quantities. Accordingly, residual TX-100 presence in vaccine formulations has implications for both formulation stability and safety, necessitating both accurate screening during processing to guide decision-making about filtration repeats and accurate quantitation in the final product. Accurate HPLC-based methods are used successfully for the latter but their use for routine screening during processing is far from ideal because they often require extensive sample preparation and are fairly slow, complicated and costly. Here, "deconstruction" of UV–Vis absorption spectra into components corresponding to different absorbing "species" is demonstrated as a novel and viable method for routine TX-100 screening in vaccine samples from different industrial processing steps. This method is fairly accurate and, more importantly, preparation-free, rapid, simple/user-friendly and comparatively inexpensive. It is evaluated in depth in terms of applicability conditions, limitations and potential for high-throughput adaptation as well as generalization to other complex biopharmaceutical formulations.

1. Introduction

Influenza's high mutation rate [1] makes it a recurring threat; annually, influenza epidemics cause an estimated 3–5 million severe illness cases and 250–500 thousand casualties worldwide [2]. Vaccination remains as the most effective measure against infection, generally being required annually for individuals who may experience severe complications if infected [2]. Addressing efficiently this annual need for vaccines and the potential sudden need should there be a pandemic, requires the rapid release of quality vaccines into the market, which in turn requires streamlined manufacturing and quality control processes [3–5].

Most of the influenza vaccines in the market are produced using chicken eggs [5–7] and contain remnant antigens from "split" viruses [3–5,8–10]. Such split-virus vaccines are sufficiently immunogenic and tend to be considerably less reactogenic than whole virus vaccines [3,8,10,11]. Splitting, which is typically preceded by inactivation treatments, is achieved using a surfactant [1,3–6,8–10,12,13]; perhaps the most common surfactant used for this purpose is Triton X-100 (TX-100) [3,10,12].

TX-100 is not known to denature the viral proteins [3]; this makes it useful for maintaining their conformational stability in the relatively destabilizing environment they may find themselves in following virus splitting. Maintaining the antigens' 3-D conformational structure is important not only for proper priming of the immune system against the pathogen [3] but also for curbing unwanted protein aggregation phenomena. Accordingly, TX-100, like some other surfactants, can aid to partially stabilize protein-abundant formulations like vaccines against protein aggregation [1,6,8–10,14–16]. This is especially important considering large

Abbreviations: TX-100, Triton X-100; RP-HPLC, reverse-phase high-performance liquid chromatography; UV–Vis, ultraviolet-visible; FDA, Food and Drug Administration (USA); PS1, processing step 1; PS2, processing step 2; PBS, phosphate-buffered saline; NATA, N-acetyl-L-tryptophanamide; RNA, ribonucleic acid; Trp, tryptophan; Tyr, tyrosine; Nt, nucleotide; DNA, deoxyribonucleic acid.

* Corresponding author at: The University of Sydney, School of Pharmacy, Science Rd, Pharmacy & Bank Building (A15), Rm S242, NSW 2006, Australia
E-mail addresses: ziya.sahin@sydney.edu.au (Z. Sahin), Ronald.Neeleman@sanofipasteur.com (R. Neeleman), Jonathan.Haines@sanofipasteur.com (J. Haines), veysel.kayser@sydney.edu.au (V. Kayser).

https://doi.org/10.1016/j.vaccine.2018.12.069
0264-410X/

protein aggregates can be a serious concern for formulation stability (because their extensive formation may lead to protein precipitation) [3,7,8,14,16–21] and possibly safety [7,13,14,16,17,19,21–25]. Since protein aggregation can occur at almost every stage of processing, TX-100′s aggregation-curbing ability makes it beneficial for formulation stability and safety, although this ability is not the primary reason for its use in vaccine manufacturing.

TX-100′s positive stabilizing property is countered by its toxicity in large quantities [26,27]. As a result, after splitting has been achieved, its concentration must be reduced to residual levels below limits specified and regulated by health administration authorities, so that it does not pose a health risk [10]. Ultimately, TX-100 content in the final product needs to be optimized to ensure the formulation is both safe and relatively stable against aggregation. While the former can be achieved by keeping the TX-100 concentration significantly below toxicity levels (all manufacturers keep it below 500 μg/mL, which is significantly lower than even levels with insignificant toxic effects in mice [26,27]), the latter can be achieved by keeping a high surfactant to protein ratio in the formulation [4,8,10,16]. Thus, it is necessary not only to accurately quantitate TX-100 in the final formulation but also to accurately and routinely screen TX-100 concentration during processing so that decisions can be made regarding the number of filtration runs [10].

TX-100 quantitation in vaccines is usually achieved using HPLC-based methods [10,16,28]. Though they are accurate, these methods often require extensive sample preparation and are quite slow, complicated and costly, making them far from ideal for efficient routine screening during processing. Therefore, there is a need for novel, accurate screening methods that are relatively free from ideally all of the limitations mentioned above. Such methods can facilitate more efficient quality control throughout processing and thus accelerated vaccine release. A UV–Vis absorption-based quantitation method that is fairly free from most of the above limitations has been reported [10]. The method calls for the isolation of TX-100 from the formulation before analysis, due to the heavy overlap between TX-100′s spectrum and the spectra of other "species" found in vaccine formulations (certain amino acids in proteins [8,29], genetic material from viruses, etc.). However, since absorbance is additive [30–32], TX-100's concentration can actually be calculated fairly accurately from the mixture's spectrum, eliminating extra sample preparation steps like isolation for the purposes of highly rapid screening.

Using the additivity of absorbance, the absorption spectrum of a complex system can be "deconstructed" into components corresponding to the constituent absorbing species, provided relevant controls are done to identify the individual spectral behavior of each species and possible spectrum-altering factors are negligible or addressable [30–32]. Here, the application of this method to influenza split-virus vaccine samples from two different industrial processing steps is shown to demonstrate the fairly accurate and, more importantly, preparation-free, rapid, simple/user-friendly and comparatively inexpensive screening of TX-100 content in vaccine formulations. The screening accuracy was verified through comparison of the calculated concentrations to concentrations measured with an FDA-approved RP-HPLC method.

2. Materials and methods

2.1. Materials

All 24 influenza pre-vaccine samples were provided by Sanofi-Pasteur (Pennsylvania, USA). The samples were from 12 different processing batches. In each batch, two samples corresponding to two different industrial processing steps were extracted; the processing steps are named processing step 1 (PS1) and 2 (PS2) here, respectively. Each batch was produced using one of the following strains: A/California/7/2009 (H1N1) [batches 7 and 12], A/South Australia/55/2014 (H3N2) [batches 1, 2 and 8], A/Switzerland/9715293/2013 (H3N2) [batches 9 and 10], B/Brisbane/60/2008 (H3N2) [batches 5, 6 and 11] and B/Phuket/3073/2013 (H3N2) [batches 3 and 4]. All the samples were kept at 2–8 °C during storage and shipment.

PBS tablets, TX-100 (laboratory grade) and N-acetyl-L-tryptophanamide (NATA) were purchased from Sigma-Aldrich (New South Wales, AUS) and used as received. A PBS solution in deionized water (0.01 M, pH 7.4) was prepared and used for all TX-100 and NATA control sample preparations as well as vaccine sample dilutions. Mixing was performed by gentle pipetting to avoid possible, undesirable protein aggregation phenomena [16,18,19]. For all spectroscopy experiments, a Hellma quartz microcuvette (New York, USA) with a path length of 0.3 cm was used. Data was analyzed with Igor Pro 6 (Oregon, USA) and Microsoft Excel 2010 (New South Wales, AUS).

2.2. HPLC

An FDA-approved RP-HPLC protocol was followed for TX-100 quantitation in all the pre-vaccine samples. This protocol has previously been described [16].

2.3. UV–Vis absorption spectroscopy

UV–Vis absorption by the samples was measured from 200 to 400 nm using 0.5 nm slits on a Shimadzu 2600 UV–Vis spectrophotometer (New South Wales, AUS). Measurements were conducted at room temperature immediately after samples were removed from storage. Each scan was performed at least twice and the spectra averaged. 3 separate aliquots were tested for each sample (n = 3). Necessary corrections were performed for all spectra. The method used to correct some spectra for light scattering before screening analysis has previously been described [16,32].

For screening analysis, absorbance values at given wavelengths were deconstructed into components corresponding to different absorbing species using the following overall equation (Eq. (1)):

$$\begin{aligned} A_{X(\text{Total})} &= A_{X(\text{Species 1})} + A_{X(\text{Species 2})} + \dots \\ &= \{\varepsilon_{X(\text{Species 1})} * [\text{Species 1}] * L\} + \{\varepsilon_{X(\text{Species 2})} * [\text{Species 2}] * L\} + \dots \end{aligned} \quad (1)$$

where A is absorbance, X is a given wavelength, ε is extinction coefficient and L is the path length.

3. Results and discussion

The additivity of absorbance was verified through control experiments performed using mixtures of TX-100 and NATA in PBS solution. The representative spectra in Fig. 1A show this additivity, since the spectrum obtained through direct addition (blue diamonds) of a TX-100 spectrum (500 μg/mL) (grey crosses) and an NATA spectrum (250 μg/mL) (red squares) overlaps extremely well with the spectrum for a 1:1 mixture (black circles) of TX-100 (1000 μg/mL) and NATA (500 μg/mL) (final concentrations are thus 500 and 250 μg/mL, respectively). The negligible deviation from perfect overlap is expected given the unavoidable, slight variations in measurement associated with such instruments. Admittedly, many biopharmaceutical formulations are much more complex in composition than these control mixtures, leading to more complex spectra that are often affected by factors like hypo/hyperchromicity and light scattering. Despite this, the principle still applies so long as the constituent absorbing species

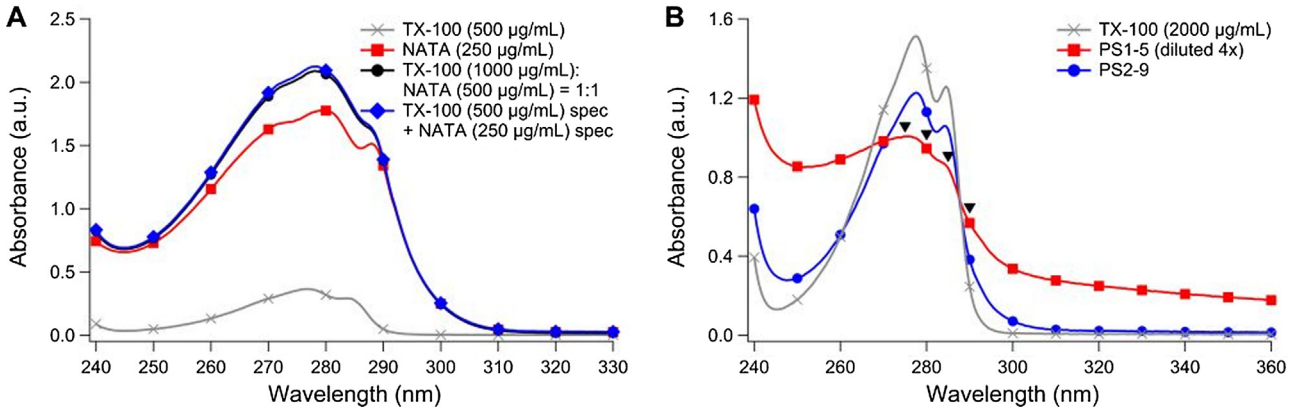

Fig. 1. (A) Representative absorption spectra showing absorbance additivity, since direct addition of the individual TX-100 (grey crosses) and NATA (red squares) spectra results in the blue spectrum (diamonds) that overlaps almost perfectly with the spectrum of a corresponding mixture (black circles). (B) Representative absorption spectra for a TX-100 sample in PBS solution (grey crosses), a typical vaccine sample from PS1 (red squares) and a typical vaccine sample from PS2 (blue circles). PS1 samples were all diluted 4-fold. Significant light scattering above 320 nm can be seen for the PS1 sample but not for the PS2 sample; the same was true for all the other PS1 and PS2 samples (not shown). The black triangles indicate the wavelengths (275, 280, 285 and 290 nm) at which absorbance values were taken for screening analysis. (For interpretation of the references to colour in this figure legend, the reader is referred to the web version of this article.)

can be identified and such factors are negligible or can be addressed.

Fig. 1B shows representative spectra for a TX-100 sample in PBS solution (grey crosses), a typical vaccine sample from PS1 (red squares) and a typical vaccine sample from PS2 (blue circles). PS1 is higher up in the processing stream and as such, samples from this step were too concentrated for direct measurement, prompting 4-fold dilution of all of them with PBS solution. Samples from PS2 were measured as they were. As evident in Fig. 1B, significant light scattering above 320 nm was seen for PS1 samples but not for PS2 samples. As a result, PS1 sample spectra were corrected for the blank and scattering prior to screening analysis (please refer to [16] for a corrected spectrum example), while PS2 sample spectra were only corrected for the blank.

Initial screening analysis assumed significant contribution to the spectra only by TX-100 molecules and tryptophan residues in proteins. This assumption proved to be too simplistic, as most of the TX-100 concentrations calculated using it did not quite match the concentrations measured using the RP-HPLC method (results not shown). Specifically, most TX-100 concentrations were considerably overestimated, clearly due to absorbance contributions by non-modelled species being attributed to TX-100 molecules (and tryptophan residues). As a result, two more species were incorporated into analysis - tyrosine residues in proteins and nucleotides in virus RNA - necessitating absorbance values at four different wavelengths for specific solutions to the constructed simultaneous equations.

The formulations have several more absorbing species so the four wavelengths had to be in a region where these non-modelled species would have negligible to no absorbance. The wavelengths 275, 280, 285 and 290 nm (marked in Fig. 1B) were thus chosen, as species like disulfide bonds and phenylalanine residues show negligible while species like peptide bonds show no absorbance above 270 nm. However, negligible absorbance contributions are still finite and thus their incorporation into modelling, which would require an additional equation per species, will lead to more rigorous solutions. In fact, these negligible but finite contributions are amongst the reasons why some samples' spectra were not represented perfectly by the four-species system of equations; i.e. there was very slight deviation in some fits.

$$A_{X(Total)} = A_{X(TX-100)} + A_{X(Trp)} + A_{X(Tyr)} + A_{X(Nt)} \quad (2)$$

$$\therefore A_{275}/L = \{\varepsilon_{275(TX-100)} * [TX-100]\} + \{\varepsilon_{275(Trp)} * [Trp]\} + \{\varepsilon_{275(Tyr)} * [Tyr]\} + \{\varepsilon_{275(Nt)} * [Nt]\} \quad (3)$$

$$\therefore A_{280}/L = \{\varepsilon_{280(TX-100)} * [TX-100]\} + \{\varepsilon_{280(Trp)} * [Trp]\} + \{\varepsilon_{280(Tyr)} * [Tyr]\} + \{\varepsilon_{280(Nt)} * [Nt]\} \quad (4)$$

$$\therefore A_{285}/L = \{\varepsilon_{285(TX-100)} * [TX-100]\} + \{\varepsilon_{285(Trp)} * [Trp]\} + \{\varepsilon_{285(Tyr)} * [Tyr]\} + \{\varepsilon_{285(Nt)} * [Nt]\} \quad (5)$$

$$\therefore A_{290}/L = \{\varepsilon_{290(TX-100)} * [TX-100]\} + \{\varepsilon_{290(Trp)} * [Trp]\} + \{\varepsilon_{290(Tyr)} * [Tyr]\} + \{\varepsilon_{290(Nt)} * [Nt]\} \quad (6)$$

Eq. (2) is the overall equation for deconstruction of the absorbance at a given wavelength into four components corresponding to the four absorbing species modelled. Dividing throughout by the path length and using the wavelengths 275, 280, 285 and 290 nm produces Eqs. (3)–(6). The extinction coefficients at the chosen wavelengths can be derived from control experiments performed using a given absorbing species in isolation in the formulation medium; Fig. 2 shows an example of this for TX-100 in PBS solution.

Fig. 2A shows representative spectra for a TX-100 dilution series in PBS solution from 2000 to 100 µg/mL in 100 µg/mL increments. Three separate aliquots were measured for each concentration and absorbance values at the chosen wavelengths were taken each time. Plotting these values like in Fig. 2B allowed accurate calculation of the molar extinction coefficient at each wavelength for TX-100 in PBS solution. Similar control experiments can be done for the other absorbing species using representative analogues, such as NATA for tryptophan residues. For the purposes of this study, the extinction coefficients for TX-100 and tryptophan residues were calculated from such control experiments but those for tyrosine residues and nucleotides (the two species incorporated later) were taken or deduced from the literature (discussed below). Once the extinction coefficients were calculated, the only unknowns in Eqs. (3)–(6) were the concentrations of the four absorbing species, allowing specific solutions.

The molar extinction coefficients for TX-100 were calculated to be (Fig. 2B): 275 nm–1501; 280 nm–1397; 285 nm–1283; 290 nm–234. For tryptophan residues, an NATA dilution series in PBS solution was used to calculate the molar extinction coefficients as: 275 nm–5384; 280 nm–5554; 285 nm–4800; 290 nm–4283. Based on their extensive statistical analysis, Mach and co-workers determined an average value of 5540 as the molar extinction coefficient at 280 nm for tryptophan in native proteins [33]; since this value is in excellent agreement with the one determined

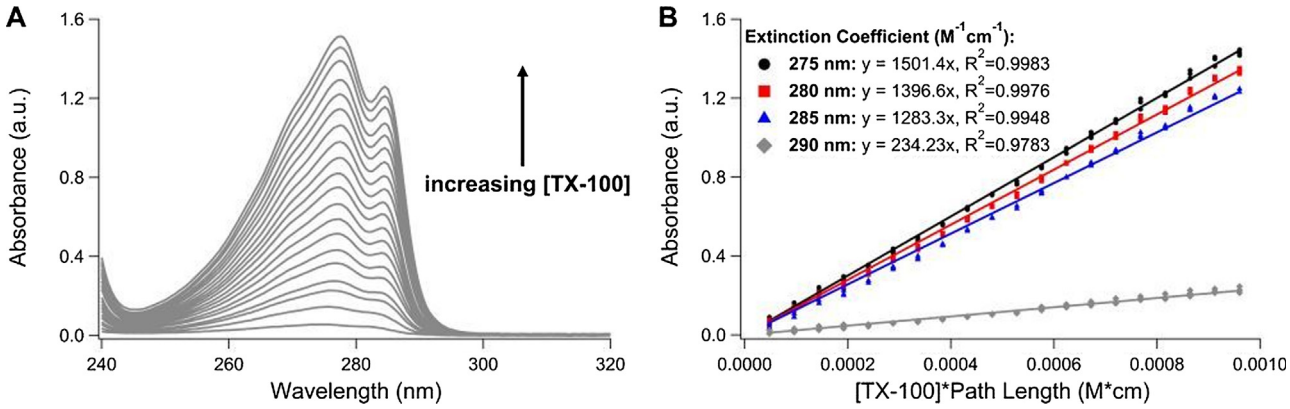

Fig. 2. (A) Representative absorption spectra for TX-100 samples in PBS solution. The samples had TX-100 concentrations ranging from 100 to 2000 μg/mL in 100 μg/mL increments. The path length was 0.3 cm. (B) Linear plots used to calculate the extinction coefficient for TX-100 in PBS solution at 275, 280, 285 and 290 nm. The data points were derived from spectra like those in A. At each wavelength, for each x value, there are three absorbance values derived respectively from the spectra for three separate aliquots tested for each concentration (n = 3). The lines show linear fits to the data points for each wavelength, with the y-intercept set to 0 in each case. Following the Beer-Lambert Law, the gradient for each line corresponds to the extinction coefficient (in M^{-1} cm^{-1}) at that wavelength; these values were used for subsequent screening analysis.

here, the extinction coefficients obtained from the NATA dilution series were deemed reflective of the absorption of tryptophan residues in the formulations studied.

Tyrosine residues and nucleotides were not included in initial analysis due to the assumption that they did not contribute significantly to the spectra because of minute concentrations. Accordingly, their incorporation afterwards was based on coarse determination of their extinction coefficients as this was deemed sufficient for demonstrating the expected improvement in TX-100 screening. For tyrosine residues, an average molar extinction coefficient of 1480 at 280 nm was given by Mach and co-workers [33]. Based on a tyrosine analogue, tyrosine absorbance at 275, 285 and 290 nm is roughly 0.83, 0.90 and 0.62, respectively, if absorbance at 280 nm is 1 [34]. Using these ratios in tandem with the abovementioned value at 280 nm, the following coarse molar extinction coefficients were obtained: 275 nm–1224; 280 nm–1480; 285 nm–1338; 290 nm–911. For a nucleotide in a long, essentially randomized nucleotide sequence, the commonly used average extinction coefficient at 260 nm is 8000 M^{-1} cm^{-1} [31]. If absorbance at 260 nm is 1, coarse absorbance for pure, single-stranded RNA at 275, 280, 285 and 290 nm is 0.70, 0.48, 0.32 and 0.22, respectively [35]. Using these values together, the following coarse molar extinction coefficients were obtained for nucleotides in influenza RNA: 275 nm–5600; 280 nm–3840; 285 nm–2560; 290 nm–1760.

Using the derived extinction coefficients in Eqs. (3)–(6) produced the results in Table 1 for TX-100 concentration in PS1 and PS2 samples. The second and third columns show the average TX-100 concentrations as measured by RP-HPLC and as calculated through four-species fitting to absorption spectra, respectively. The accuracy of the screening is evident, with less than 15% error (and underestimation) for most of the PS1 samples and less than 10% error (and overestimation) for all the PS2 samples. As mentioned earlier, PS1 is higher up in the processing stream, making samples from this step more complex in composition than PS2 samples; this added complexity was evident from not only the significant light scattering seen in the spectra of PS1 samples (Fig. 1B) but also the often larger percent errors in TX-100 screening for these samples (Table 1).

The fairly systematic underestimation for PS1 samples and systematic overestimation for PS2 samples are largely associated with light scattering contributions to the spectra. With respect to the PS1 samples' spectra, which were corrected for scattering, it seems that the correction approach used is slightly overestimating light scattering contributions, resulting in the elimination of some absorbance reading due to genuine absorption events and thus leading to the slight underestimation of TX-100 content in almost all the samples tested. With respect to the spectra of the PS2 samples, even though they did not show significant scattering above 320 nm and were not corrected as a result, it would be wrong to claim that scattering did not at all contribute to their measurement. Accordingly, the slight overestimation of TX-100 content in all the PS2 samples studied is largely the result of such small but nonetheless finite scattering contributions passing off as absorbance due to genuine absorption events. The systematic error in both these cases can thus be addressed by improving scattering correction.

Table 1
Comparison of the TX-100 concentrations calculated through four-species fitting to absorption spectra with those obtained using the FDA-approved RP-HPLC method. Four-species fitting was able to capture, in most cases and for the most part, the complexity of the samples' spectra.

Sample	RP-HPLC	UV–Vis Absorption – 4 Species Fit	
	Average [TX-100] (μg/mL)	Average [TX-100] ± SD (μg/mL)	% Error
PS1-1	1411	1257 ± 58	−11
PS1-2	1187	968 ± 14	−18
PS1-3	1324	1119 ± 9	−15
PS1-4	1287	1131 ± 19	−12
PS1-5	1510	1416 ± 111	−6
PS1-6	1403	1244 ± 67	−11
PS1-7	1497	1299 ± 11	−13
PS1-8	1374	1346 ± 46	−2
PS1-9	1538	1364 ± 70	−11
PS1-10	1351	1213 ± 41	−10
PS1-11	1734	1806 ± 77	4
PS1-12	1492	1344 ± 37	−10
PS2-1	587	629 ± 16	7
PS2-2	568	601 ± 23	6
PS2-3	737	773 ± 20	5
PS2-4	675	722 ± 12	7
PS2-5	562	592 ± 3	5
PS2-6	466	472 ± 4	1
PS2-7	1031	1123 ± 15	9
PS2-8	572	592 ± 5	4
PS2-9	1165	1179 ± 6	1
PS2-10	1097	1153 ± 5	5
PS2-11	1221	1299 ± 18	6
PS2-12	951	978 ± 8	3

Importantly, the lowest concentration of TX-100 tested and quantitated here was 100 μg/mL (Fig. 2A) but UV–Vis absorption spectroscopy has been shown to be able to quantitate and detect TX-100 down to 3 and 1 μg/mL, respectively [10]. Therefore, given that the lowest reported concentration of TX-100 in a commercial influenza split-virus vaccine formulation is around 170 μg/mL [10] and that the method herein is actually intended for screening samples higher up in the processing stream (i.e. with higher TX-100 content than the final formulations), there should be no issue with respect to the method's ability to screen samples with lower TX-100 content than the 24 samples tested here (Table 1). Overall, the values obtained by fitting four absorbing species to the spectra and the minor percent errors associated with them clearly demonstrate the viability of this preparation-free, rapid, user-friendly and comparatively inexpensive method for fairly accurate screening of TX-100 content in influenza vaccine samples from different industrial processing steps.

For complex formulations like the influenza vaccine samples used in this study, modelling of UV–Vis absorption spectra with four absorbing species, although managing to produce quite good results in this wavelength range, is admittedly not exhaustive. As such, incorporating other contributing species into modelling, however small their contribution to the spectra may be, will improve the accuracy of screening, as evident from the two- and four-species fitting findings reported above. On this note, experiments can be done to identify other potential absorbing species in the vaccine formulation that contribute to the spectra in the chosen wavelength range. Ideally, incorporation of each species should be based on relevant control experiments to determine its individual spectral behavior in the specific formulation medium, as was done here for TX-100 and tryptophan residues through dilution series. This would ensure deduction of more accurate extinction coefficients, which would also ensure more accurate screening.

A few factors need consideration with regards to modelling of the biological absorbing species. Firstly, since influenza split-virus vaccine formulations can have a large variety of proteins and RNA segments, using the fundamental absorbing units in biological constituents (i.e. amino acids and nucleotides rather than whole proteins and RNA segments, respectively) for modelling is the easiest, most convenient and most flexible but possibly not the most accurate way of approaching deconstruction of the spectra. The "fundamental unit approach" is more feasible because, alongside purification issues for the RNA segments, finding the formulation-medium-specific extinction coefficients at several wavelengths for such a variety of proteins and RNA segments would be extremely tedious. However, the fundamental unit approach may not be able to take into account conformation-related factors that can affect the extinction coefficient of nucleotides and, to a minute degree, amino acids.

Specifically, due to base-stacking effects, the extinction coefficient for a nucleotide sequence will always be less than the addition of the extinction coefficients of the constituent nucleotides [36–39]. Thus, the fundamental unit approach for RNA nucleotides essentially follows the simpler and more flexible "base composition method" (adding the extinction coefficients for isolated nucleotides) for oligonucleotide extinction coefficient prediction, rather than the more accurate but often inconvenient "nearest neighbor method", which takes into account base-stacking and base-sequence effects by also considering interactions between adjacent bases in calculation [36–39]. The fundamental unit approach, therefore, can potentially result in overestimation of RNA extinction coefficients and hence RNA contribution to the spectra.

Moreover, although hypo/hyperchromicity is a phenomenon identified more with double-stranded DNA than RNA, the possibility of some hypochromicity in RNA segments due to self-complementarity-based "folding" (i.e. further base stacking) and the consequent reduction in extinction coefficients should not be ruled out completely [31,39]. The fundamental unit approach can also overlook this minor factor, again resulting in overestimation of RNA contribution to the spectra. Despite these points though, the well-established average extinction coefficient used for a nucleotide in a long, essentially randomized sequence (8000 M^{-1} cm^{-1} at 260 nm) [31] seems to account for these effects as it is considerably less than the average (~11000 M^{-1} cm^{-1} at 260 nm) of the values for the four common nucleotides.

Extinction coefficients for proteins are usually not complicated by such effects, as accurate values can be calculated by adding the extinction coefficients of the individual amino acids contributing to absorption at a given wavelength, provided peptide bond absorption is not also contributing at that wavelength. However, even though hypochromicity is not usually associated with proteins, the existence of solvent perturbation spectroscopy as a technique shows that amino acid extinction coefficients may be affected, albeit minimally, by changes in the polarity of their immediate environment. Thus, the possible hypo/hyperchromic effect of protein folding and aggregation on amino acid extinction coefficients may also need consideration when taking the fundamental unit approach. Overall, while the fundamental unit approach assumes there are no conformation-related changes in the extinction coefficients of nucleotides and amino acids, and, may lack in modelling accuracy as a result, it can be reliably used if such changes are negligible or can be addressed via evidence-based correction of the derived or predicted extinction coefficients [31,37].

Secondly, solution properties like ionic strength, pH and temperature can also affect the extinction coefficients of proteins and RNA [31,40,41] by influencing their folding/unfolding and thus conformational structure. This again highlights the importance not only of deriving extinction coefficients from the results of control experiments conducted with the specific formulation medium but also of keeping samples refrigerated during storage and taking measurements either at the refrigeration temperature or at room temperature immediately after removal from storage. Accordingly, the coarse extinction coefficients derived herein for tyrosine residues and RNA nucleotides based on values and absorbance ratios from the literature may need revision based on control experiments, since they will not necessarily be reflective of the conditions in the formulation medium for these samples (the values and ratios may be slightly different).

Finally, the spectra of some samples can be affected considerably by light scattering contributions [31,32,42], which can be an issue for accurate modelling. Large particles in vaccine formulations, especially protein aggregates, can scatter light considerably, causing significant absorbance readings above ~320 nm where proteins do not readily absorb [8,14,16,17,29,42]. Spectra that are affected by such scattering have distorted baselines and thus need to be corrected prior to screening analysis for accurate results [32]. Different methods have been developed to correct for light scattering [16,31,32,42] but due to the complex nature of the phenomenon, especially its complex dependence on scatterer size and shape, a method that works well with one particular biopharmaceutical formulation may not work well with another, especially if the samples differ significantly in particle sizes and shapes.

Here, we have used a previously described empirical approach [16,32] to correct only the spectra of PS1 samples for scattering, since PS2 samples did not show significant scattering above 320 nm (Fig. 1B). An empirical approach was used, as opposed to approaches based on the Rayleigh approximation or Mie theory [31,32,43,44], because the assumptions made about particle mean size, size distribution and shape in those approaches are not really suitable for complex formulations like the split-virus vaccine sam-

ples studied, which are quite non-uniform in terms of particle size and shape. Specifically, in the samples, particle size dimensions range from several nanometers (e.g. individual protein molecules) to a few micrometers (e.g. large, amorphous protein aggregates), while particle shape is varied and often not spherical [16]. Overall, based on the 4-species screening results for PS1 samples (Table 1), it can be said that although the empirical approach does well in correcting the spectra of these samples for scattering, it would be worthwhile to check for improvements in it using different fitting functions (a third-order polynomial was used here [16]) and to compare it to other approaches for verification of the best approach for these and similar complex samples.

4. Conclusions

Deconstruction of UV–Vis absorption spectra into components enables fairly accurate, preparation-free, rapid, user-friendly and relatively inexpensive screening of TX-100 content in influenza split-virus vaccine samples from different industrial processing steps. Once the necessary control experiments, correction tests and cross-method validation studies (all of which would take a few weeks at most) are done, this method can be used in industrial settings to facilitate efficient routine screening during processing and thus quicker vaccine release. The screening accuracy is reliant upon identification of the absorbing species in a known, routinely produced formulation; therefore, this method is not suitable for determining the contents of a mystery formulation or reliably determining the presence/quantity of impurities in an otherwise known formulation (even though this is rare in industrial reactor settings) because many different species can have similar spectral behavior.

For samples with spectra that are known to have insignificant light scattering contributions, the method can easily be adapted for high-throughput screening; if light scattering contributions are significant, however, high-throughput may only be achieved if the scatter correction method has potential for automation alongside being accurate. Finally, the method can be generalized to many other complex biopharmaceutical formulations for screening a particular ingredient (if it absorbs light), provided that the absorbing species are identified, relevant controls are done to decipher the individual spectral behavior (extinction coefficients) of these species and spectrum-altering factors are negligible or addressable.

Acknowledgements

The research was funded by Sanofi-Pasteur. ZS acknowledges the School of Pharmacy at the University of Sydney for the postgraduate research scholarship used during this study and others. Author contributions: study conception and design – ZS, RN, JH and VK; acquisition of data – ZS, RN and JH; analysis and interpretation of data – ZS, RN, JH and VK; drafting of manuscript – ZS and VK; critical revision – ZS, RN, JH and VK; final approval of version to be published – ZS, RN, JH and VK.

Conflict of interest

ZS and VK declare that there was no conflict of interest. RN and JH are Sanofi employees and stockholders.

References

[1] Garman E, Laver G. The structure, function, and inhibition of influenza virus neuraminidase. In: Fischer WB, editor. Viral membrane proteins: structure, function, and drug design. New York: Kluwer Academic/Plenum Publishers; 2005. p. 247–67.
[2] Fact sheet: Influenza (Seasonal). [Internet] 2014 March [cited 2015 December]; about 3 screens. Available from: http://www.who.int/mediacentre/factsheets/fs211/en/.
[3] Lee KKH et al. Quantitative determination of the surfactant-induced split ratio of influenza virus by fluorescence spectroscopy. Hum Vaccines Immunother 2016:1–9.
[4] Belanger JM et al. Orthogonal inactivation of influenza and the creation of detergent resistant viral aggregates: towards a novel vaccine strategy. Virol J 2012;9(72).
[5] Huckriede A et al. The virosome concept for influenza vaccines. Vaccine 2005;23:S26–38.
[6] Ruigrok RWH et al. Electron microscopy of the low pH structure of influenza virus hemagglutinin. EMBO J 1986;5(1):41–9.
[7] Patois E et al. Stability of seasonal influenza vaccines investigated by spectroscopy and microscopy methods. Vaccine 2011;29(43):7404–13.
[8] Tay T et al. Investigation into alternative testing methodologies for characterization of influenza virus vaccine. Hum Vaccines Immunother 2015;11(7):1673–84.
[9] Hoyle L, Barker SM. Fractionation of the influenza virus with the object of producing subunit vaccine. Postgrad Med J 1973;49(569):193–4.
[10] Pavlovic B et al. Direct UV spectrophotometry and HPLC determination of Triton X-100 in split virus influenza vaccine. J AOAC Int 2016;99(2):396–400.
[11] Webster RG et al. Potentiation of the immune response to influenza virus subunit vaccines. J Immunol 1977;119(6):2073–7.
[12] Ruigrok RWH, Calder LJ, Wharton SA. Electron microscopy of the influenza virus submembranal structure. Virology 1989;173(1):311–6.
[13] Babiuk S et al. Aggregate content influences the Th1/Th2 immune response to influenza vaccine: evidence from a mouse model. J Med Virol 2004;72(1):138–42.
[14] Wang W. Protein aggregation and its inhibition in biopharmaceutics. Int J Pharm 2005;289(1–2):1–30.
[15] Manning MC et al. Approaches for increasing the solution stability of proteins. Biotechnol Bioeng 1995;48(5):506–12.
[16] Sahin Z et al. Nile Red fluorescence spectrum decomposition enables rapid screening of large protein aggregates in complex biopharmaceutical formulations like influenza vaccines. Vaccine 2017;35(23):3026–32.
[17] Li Y, Mach H, Blue JT. High throughput formulation screening for global aggregation behaviors of three monoclonal antibodies. J Pharm Sci 2011;100(6):2120–35.
[18] Sahin Z, Demir YK, Kayser V. Global kinetic analysis of seeded BSA aggregation. Eur J Pharm Sci 2016;86:115–24.
[19] Kayser V et al. Evaluation of a non-Arrhenius model for therapeutic monoclonal antibody aggregation. J Pharm Sci 2011;100(7):2526–42.
[20] Maddux NR et al. High throughput prediction of the long-term stability of pharmaceutical macromolecules from short-term multi-instrument spectroscopic data. J Pharm Sci 2014;103(3):828–39.
[21] Demeule B et al. New methods allowing the detection of protein aggregates: a case study on trastuzumab. Mabs 2009;1(2):142–50.
[22] Purohit VS, Middaugh CR, Balasubramanian SV. Influence of aggregation on immunogenicity of recombinant human factor VIII in hemophilia A mice. J Pharm Sci 2006;95(2):358–71.
[23] Schellekens H. Bioequivalence and the immunogenicity of biopharmaceuticals. Nat Rev Drug Discovery 2002;1(6):457–62.
[24] Rosenberg AS. Effects of protein aggregates: an immunologic perspective. AAPS J 2006;8(3):E501–7.
[25] Braun A et al. Protein aggregates seem to play a key role among the parameters influencing the antigenicity of interferon alpha (IFN-alpha) in normal and transgenic mice. Pharm Res 1997;14(10):1472–8.
[26] Cornforth JW et al. Antituberculous effect of certain surface-active polyoxyethylene ethers in mice. Nature 1951;168(4265):150–3.
[27] Horowitz B et al. Solvent detergent-treated plasma – a virus-inactivated substitute for fresh-frozen plasma. Blood 1992;79(3):826–31.
[28] Heinig K, Vogt C. Determination of Triton X-100 in influenza vaccine by high-performance liquid chromatography and capillary electrophoresis. Fresenius J Anal Chem 1997;359(2):202–6.
[29] Capelle MAH, Arvinte T. High-throughput formulation screening of therapeutic proteins. Drug Disc Today Technol 2008;5(2–3):e71–9.
[30] Kalb VF, Bernlohr RW. A new spectrophotometric assay for protein in cell extracts. Anal Biochem 1977;82(2):362–71.
[31] Porterfield JZ, Zlotnick A. A simple and general method for determining the protein and nucleic acid content of viruses by UV absorbance. Virology 2010;407(2):281–8.
[32] Mantele W, Deniz E. UV-VIS absorption spectroscopy: lambert-beer reloaded. Spectrochimica Acta Part A – Mol Biomol Spectrosc 2017;173:965–8.
[33] Mach H, Middaugh CR, Lewis RV. Statistical determination of the average values of the extinction coefficients of tryptophan and tyrosine in native proteins. Anal Biochem 1992;200(1):74–80.
[34] Balestrieri C et al. Second-derivative spectroscopy of proteins: a method for the quantitative determination of aromatic amino acids in proteins. Eur J Biochem 1978;90(3):433–40.
[35] Switzer RL, Garrity LF. Experimental biochemistry: theory and exercises in fundamental methods. 3rd ed. New York: W. H. Freeman; 1999.
[36] Cantor CR, Warshaw MM, Shapiro H. Oligonucleotide interactions. 3. Circular dichroism studies of the conformation of deoxyoligonucleotides. Biopolymers 1970;9(9):1059–77.
[37] Cavaluzzi MJ, Borer PN. Revised UV extinction coefficients for nucleoside-5'-monophosphates and unpaired DNA and RNA. Nucleic Acids Res 2004;32(1):1–9.

[38] Kallansrud G, Ward B. A comparison of measured and calculated single- and double-stranded oligodeoxynucleotide extinction coefficients. Anal Biochem 1996;236(1):134–8.
[39] Murphy JH, Trapane TL. Concentration and extinction coefficient determination for oligonucleotides and analogs using a general phosphate analysis. Anal Biochem 1996;240(2):273–82.
[40] Mueller F, Mayhew SG, Massey V. On the effect of temperature on the absorption spectra of free and protein-bound flavines. Biochemistry 1973;12(23):4654–62.
[41] Varkonyi Z, Kabok K. Effect of temperature on light-absorption and fluorescence of the peroxidase. Acta Biochimica et Biophysica Academiae Scientiarum Hungaricae 1975;10(1–2):129–37.
[42] Leach SJ, Scheraga HA. Effect of light scattering on ultraviolet difference spectra. J Am Chem Soc 1960;82(18):4790–2.
[43] Cox AJ, DeWeerd AJ, Linden J. An experiment to measure Mie and Rayleigh total scattering cross sections. Am J Phys 2002;70(6):620–5.
[44] Drake RM, Gordon JE. Mie scattering. Am J Phys 1985;53(10):955–62.